Structural, dynamical, and electronic properties of the ionic liquid 1-ethyl-3-methylimidazolium bis(trifluoromethylsulfonyl)imide

Kana Ishisone, Guido Ori, Mauro Boero

Structural, dynamical, and electronic properties of the ionic liquid 1-Ethyl-3-methylimidazolium bis(trifluoromethylsulfonyl)imide

Kana Ishisone, Guido Ori, Mauro Boero

University of Strasbourg, Institut de Physique et Chimie des Matériaux de Strasbourg, CNRS, UMR 7504, 23 rue du Loess, F-67034 France

KEYWORDS. First Principles, Molecular Modeling, Ionic Liquids.

ABSTRACT

We provide an atomistic insight into the multifold interactions occurring in the ionic liquid 1-Ethyl-3-methylimidazolium bis(trifluoromethylsulfonyl)imide [EMIM] [TFSI] currently targeted for applications in next-generation low-power electronics and optoelectronic devices. To date, practical applications are still hampered by the lack of fundamental understanding of the interactions occurring both inside the IL and at the interface with the substrate. Our first principles dynamics simulations provide accurate structural, dynamical and electronic properties

at an atomic level of this ionic liquid, so far not yet completely unraveled. Mobilities of the two ionic species are obtained via long-lasting dynamical simulations at finite temperature, allowing for a simultaneous monitoring and quantification of the isomerization occurring in the IL. Moreover, a thorough analysis of the electronic structure and partial charges distribution characterizing the two components, cation and anion, allow rationalizing the nature of the electrostatic interactions, hydrogen bonding properties of the two ionic counterparts and the infra-red and dielectric response of the system for a full characterization of the IL.

1. INTRODUCTION

The forefront field of device electronics based on 2D semiconducting (nano)materials such as graphene, h-BN, MoS_2, WSe_2, and black phosphorous (BP) is becoming a playground for applications in forthcoming electronic and optoelectronic devices. In this type of system, a crucial factor is the possibility of achieving a high interfacial charge density (HICD) crucial to trigger unprecedented and interesting phenomena such as superconductivity[1,2] and quantum interference (QI) effects[3]. Furthermore, HICD has been indicated as a key factor to improve the performance of emerging memory devices technologies for neuromorphic computing[4,5]. In this general scenario, ionic liquids (ILs) are becoming major component to pioneer novel 2D materials-based field-effect transistors, which could greatly benefit from a gating capable of inducing a HICD, as the latter would allow to reduce the operating voltages[1-6] with clear advantages in terms of energy consumption and sustainability. From a general point of view, ILs are compounds made of a liquid salt containing mobile organic cations and inorganic anions and their use as effective gating media has already been pioneered and fully acknowledged[5-9]. Under

an applied voltage, the ionic moieties composing the IL undergo a separation, and one of the two ionic species, either cations or anions, depending on the local electric field, accumulate on the 2D material surface, forming an electric double layer (EDL). In turn, the charge density that can be induced at the hybrid interface becomes orders of magnitude larger than that of a conventional silicon back gate. Despite intensive experimental efforts, accompanied on a few occasions by atomistic simulations either at a static quantum chemical level to complement experiments[10,11] or by classical molecular dynamics with ad-hoc force fields[12-14] key questions remain unanswered about the specific interactions occurring between the ILs and the 2D material. An additional difficulty is the fact that the integration of ILs in real applications is hampered by the lack of fundamental understanding of the interactions occurring at a molecular and atomic level. This is even more crucial in the case of ILs which exist in a liquid phase at room temperature, hence presenting all the operational problems linked to fluidity-related instability. Moreover, ILs also offer an additional advantage as "green" and recyclable solvents for chemical synthesis and can be used to develop of hybrid organic-inorganic materials in which they are confined inside the porous network of an inorganic framework[15-17]. As such, in view of the concerns about sustainability, ILs are prone to have a moderate environmental impact in terms of toxicity and biodegradability.[18,19.]

By using a first-principles molecular dynamics (FPMD), empowered by free energy sampling techniques, when necessary, we provide a microscopic insight into the IL system, 1-Ethyl-3-methylimidazolium bis(trifluoromethylsulfonyl)imide [EMIM] [TFSI], currently targeted for forefront applications[20-23]. To date, a limited number of studies[24,25] have been published exploiting FPMD to tackle this class of systems. This is mainly due to the associated computational workload needed to model a realistic IL at the thermodynamic conditions of

typical experiments. By resorting to long-lasting dynamical simulations, we aim at unraveling the structural and dynamical properties of this IL, so far not yet investigated at this level of accuracy. Our study provides a convincing picture of the relative distances of the moieties composing the IL and their evolution as a result of the electrostatic and hydrogen bond (H-bond) interaction regulating the behavior of the liquid. The 100 ps time scale of our simulations allows a thorough analysis of the electronic structure and partial charges distribution of the two components, cation and anion, represent an insight into the nature of the electrostatic interactions and H-bonding properties not accessible to experiments, yet important for boosting this innovative research line and to unravel all the fundamental microscopic features escaping experimental probes.

2. COMPUTATIONAL METHODS

Our computational approach makes use of the FPMD within the density functional theory[26] (DFT) framework and according to the Car-Parinello[27] method as implemented in the developer's version of the CPMD[28] code. The valence-core interaction was described by norm-conserving numerical pseudopotential of the Martins-Trouiller type[29,30] and the exchange and correlation functional of Becke[31] and Lee-Yang-Parr[32] (BLYP) was complemented by a first principles evaluation of the van der Waals dispersion forces based on the Wannier functions centers[33] (WFCs) boosted by a propagation scheme[34] to reduce the computational burden. Valence electrons are treated explicitly and their wavefunctions are expanded on a plane-wave (PW) basis set with a cut-off of 100 Ry. This value was accurately tuned based on the convergence of the stress tensor (pressure) as a function of the number of PWs done in the

preparation phase before starting the production run. Canonical NVT simulations were done by controlling the temperature via a Nosé-Hoover[35-37] thermostat and for the numerical integration of the Car-Parrinello equations of motion, a fictitious electron mass of 400.0 au and a time step of 3.0 au (0.0726 fs) ensured good numerical control of the constants of motion.

Our [EMIM] [TFSI] simulated system started from a liquid in a periodically repeated cubic supercell of lateral size equal to L=20.8597 Å, amounting to 680 atoms and 1360 electrons. This system size includes twenty formula units of [EMIM] [TFSI] (see Figure 1), amounting to 20 [EMIM] cations and 20 [TFSI] anions.

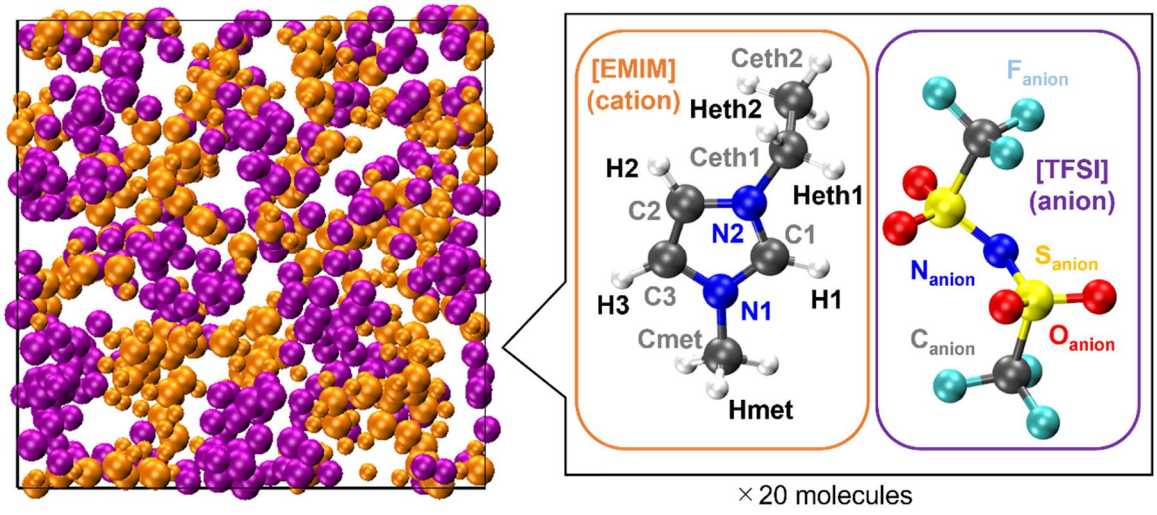

Figure 1. Simulated [EMIM] [TFSI] system (left) and detail of the ionic pair constituting the ionic liquid (right). In the left panel each cation is highlighted in orange and each anion in purple to simplify the readability of the figure. The atomic structure of a typical [EMIM] [TFSI] dimer is shown in the right panel and the atoms color code adopted here and in the following is white

for H, gray for C, blue for N, red for O, yellow for S and cyan for F. The atomic labeling and colors will be the same in the following figures.

The initial construction of the simulation cell started from the experimental density of 1.5183 g/cm^3, as reported in the literature[38,39]. On these grounds, before moving to FPMD, a classical MD simulation was used to prepare the initial configuration employing the classical force field developed by Canongia Lopes and coworkers[40], with its updated parameterization by Köddermann et al.[41].

An analysis of the internal pressure during NVT dynamics at different cell sizes allowed to optimize the reported value, which is in excellent agreement (1.5140 g/cm^3) with the experimental density and leaves the simulated system with a residual pressure oscillating around -0.4 GPa (see Fig. S1 in the *Supporting Information*), compatible with the accuracy allowed by DFT simulations[42,43]. Additional computational details will be given in the next paragraphs whenever needed to support the discussion.

3. RESULTS AND DISCUSSION

3.1 Structural properties

The complexity of this IL system makes FPMD simulations computationally demanding. The large steric volume occupied by each ion and the non-trivial molecular structure require long simulation times to reach the thermal equilibrium (see Figure S1 in the *Supporting Information*

for additional details). For this reason, we performed a ~130 ps long NVT dynamics at the target temperature of 300 K, being the typical room temperature at which many experiments are performed[3-9], apart in the case of superconductivity, and at which devices based in ILs are expected to operate. We recall that the melting point of [EMIM][TFSI] is as 256 K[44], which means that the system it is in liquid phase at room temperature. Starting from an overall analysis of the IL as a whole, all along the trajectory generated by our long-lasting dynamics, we monitored the pair correlation functions (PCFs) of the IL using the standard formula

$$g(r) = \frac{V}{4\pi r^2 N^2} \langle \sum_i \sum_{j \neq i} \delta(r - r_{ij}) \rangle \quad (1)$$

being N the number of molecules contained in the supercell of volume $V = L^3$ and $r_{ij} = |\mathbf{R}_i - \mathbf{R}_j|$ the distance between the center of mass $\mathbf{R}_i$ of each [EMIM] cation and/or [TFSI] anion (each center of mass position is sketched in Figure S2 of the *Supporting Information*). Thus, we focus here on the cation-cation, anion-anion, and cation-anion distribution, leaving the analysis of the specific atoms composing the two moieties to a later analysis of the intra-molecular structure. The result obtained is summarized in Figure 2 and provides an insightful average picture of the IL structure. Namely, the two ionic moieties keep a minimal distance of about 3.9 Å all along the dynamics with a major distribution in the range 4.9-6.7 Å where the first shoulder and the most pronounced peak of the corresponding PCF are located (Figure 2). This is mainly regulated by the mutual electrostatic interaction and by the presence of hydrogen bonds (H-bonds) as more extensively discussed in the forthcoming section dedicated to the electronic properties. A closer inspection of the curious double peak at ~5.2 Å and ~6.1 Å present in the PCF of the [EMIM] [TFSI] has shown that indeed two different conformers contribute separately to this distribution (see Figure S3 in the *Supporting Information*).

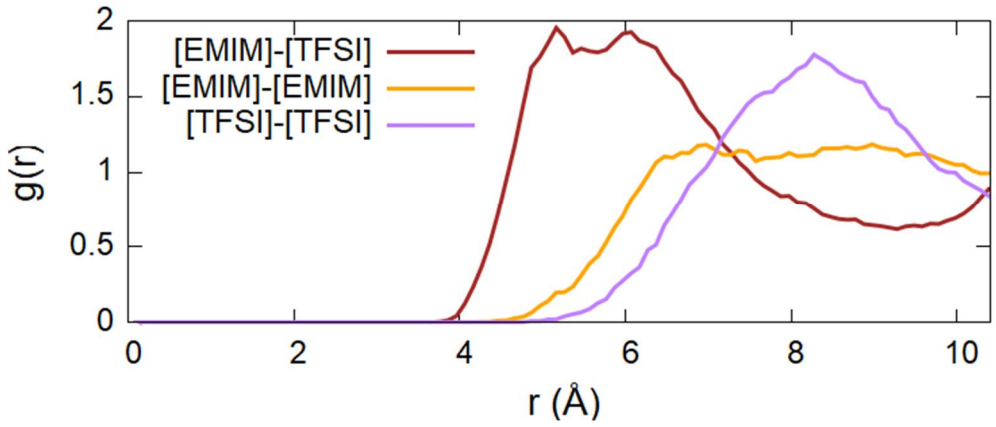

Figure 2. Pair correlation functions for the [EMIM] [TFSI] system. The brown line indicates the cation-anion radial distribution function, the orange line the cation-cation one and the purple line the anion-anion g(r).

The main features of these conformers will be detailed in the ongoing discussion. The other two PCFs, corresponding to the average cation-cation and anion-anion distribution, present broad perks between 7 and 9 Å, as expected in view of the alternance between cations and anions composing the IL. The broadening is mainly due to the flexibility of the molecular component and, in the case of the [EMIM] cations, the abundance of hydrophobic components, such as CH_3 groups, not prone to create H-bonds, makes the whole PCF distribution broad and nearly structureless. An accurate analysis of the H-bonds is presented below. A more structured peaked shape is instead present in the anion-anion distribution, since the [TFSI] exposes O and F[45] atoms which carry electrons-rich lone pairs and tend to form relatively strong H-bonds. We anticipate that these details will be clearer in the analysis of partial charges and electronic structure given in paragraph 3.3. The results summarized in Figure 2 are consistent with the ones reported in Ref. 12 obtained within a classical molecular dynamics framework.

From a more detailed atomistic standpoint, the PCFs of the single H atoms of the [EMIM] cation from the [TFSI] anion can provide additional information about the H-bond feature of the IL. This result is sketched in Figure 3, whereas other relevant interatomic distances distributions are shown in Figure S4 of the *Supporting Information*. As it can be seen from the PCF of Figure 3, rather strong H-bonds ranging from 1.6 to 3 Å (first peak of the PCF) are formed between the two ionic species and these contribute to the structure of the liquid which, indeed, is not kept together exclusively by simple Coulomb interactions between more or less distant point-like charges.

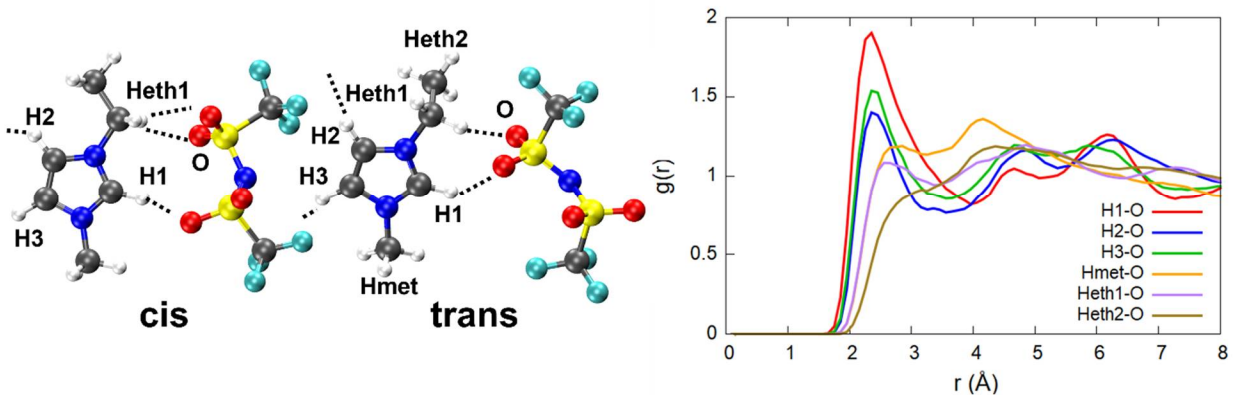

Figure 3. Trans and cis configurations spontaneously assumed by the [TFSI] in the ionic liquid (left) and pair correlation functions of the H atoms of the cation and O atoms of the anion involved in the formation of H-bonds (right). H-bonds are indicated as dashed lines and the atoms color code is identical to the one adopted in Figure 1.

An interesting feature is the fact that the anion [TFSI] can assume spontaneously either a cis or a trans orientation as sketched in Figure 3. By monitoring this feature in terms of the dihedral

angle C-S-S-C of the [TFSI] moiety all along the dynamics, we extracted the distribution presented in Figure 4. The torsion angle C-S-S-C discriminating between the cis and the trans configurations spans a range from 0º to 180º, a clear indicator of the high flexibility of the system, with a pronounced peak at 180º (trans) and a lower peak at about 40º (cis), indicating that a trans configuration is the major isomer present in the liquid all along the dynamics. The computed ratio of cis and trans conformers (regions marked in Figure 4) is 5:9.

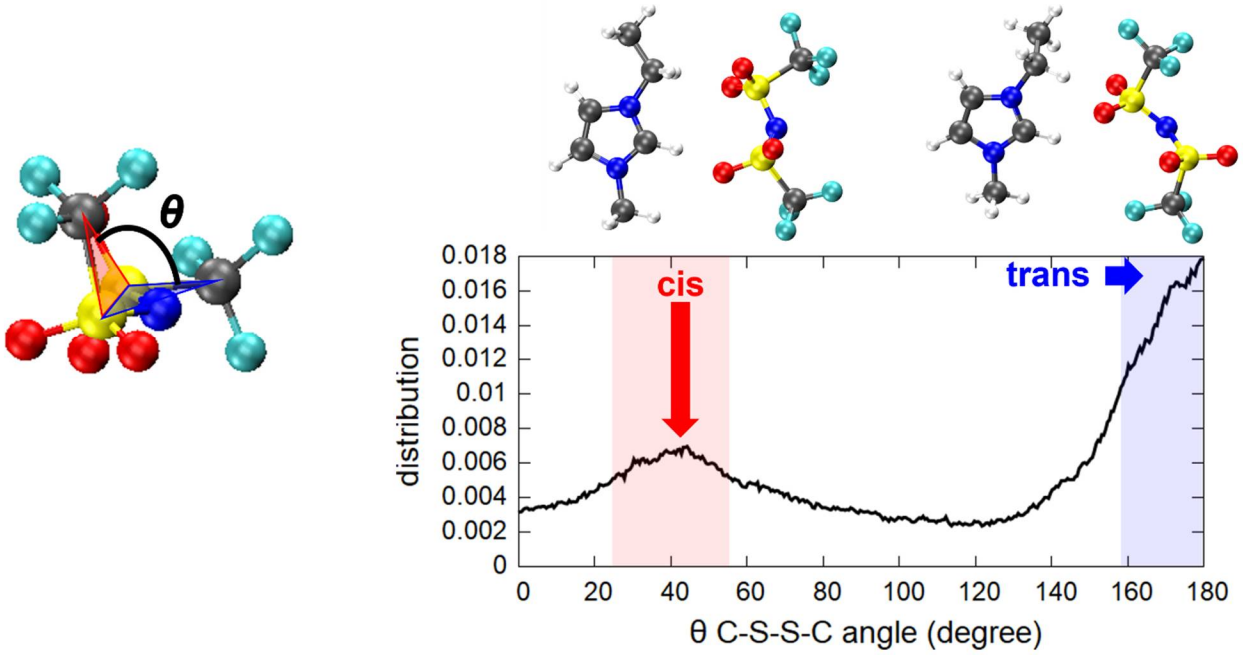

Figure 4. Distribution of the dihedral angle C-S-S-C of the [TFSI] anion, characterizing the cis-trans- isomerization during the dynamics. The colored ranges are the regions above the half height of each peak and are used to compute the cis and trans conformers ratio.

This seems to be due to the fact that a trans configuration has more degrees of freedom to form H-bonds with nearby [EMIM] cation surrounding the anion in the liquid state, without

being constrained to be bound the [EMIM] molecules shown both in Figure 3 and 4 and representing the only two possibilities in a vacuum[11]. Indeed, a full optimization of isolated [EMIM] cis-[TFSI] and [EMIM] trans-[TFSI] performed within our computational scheme in a vacuum has given a total energy difference between the two configurations of ΔE = 2.68 kcal/mol with the trans isomer energetically located above the cis one. Yet, this is due to the reduced number of H-bonds that such an isolated system can realize as a stand-alone molecular pair but does not reflect the actual situation in an extended liquid, where a wealth of possibilities in forming H-bonds (sketched in Figure 3 as dashed lines pointing outside the shown pair) exist, thus conferring a higher stability to the trans conformer, reflected in the distribution in Figure 4. This result can be ascribed to both the wide variety of H-bonding formation and to the minimization of the steric repulsion between the symmetric sulphonyl and trifluoromethyl groups promoted by the cis conformation[46]. For an IL like the one targeted in this study, 1-ethyl-3-methylimidazolium bis(trifluoromethanesulfonyl)imide, an ∼75% content of trans conformer was determined in the bulk IL using Raman spectroscopy and ab initio calculations[47]. Note that in a confined environment more efficient packing of TFSI anions is promoted by the cis conformation as found in IL confined in silica and semiconducting chalcogenide pores[17,46,48]. The distribution of the number of [EMIM] molecules having H---O H-bonds with either a cis or a trans [TFSI] in the liquid are shown in Fig. S5 of the *Supporting Information*. The trans conformer has a slightly larger number of surrounding [EMIM] molecules with respect to the cis conformer, consistent with our discussion above. Contrary to the anion, which has a very flexible (switchable) structure, the cation presents a moderate molecular flexibility, characterized by a broad distribution of the torsion angle of the C-N bond connecting the ethyl group and the imidazolium ring (θ_2 angle), with a small peak at around 100^o (out-of-plane

conformer) (Fig. S6 in *Supporting Information*). Conversely, the rigid structure of the ethyl group (Ceth2-Ceth1-N2 angle) is underscored by the sharp distribution of the θ_1 angle peaked at ~110° in the same figure.

3.2 Dynamical properties

By exploiting the 130 ps long dynamics, we focused on the mobility of the two ionic species in the IL. As done for the overall pair correlation functions in Figure 2, the centers of mass $\mathbf{R}_i(t)$ of both the [EMIM] cation and the [TFSI] anion were monitored, and the result is shown in Figure 5. We observe that the Fickian regime, namely the one in which the mean square displacement MSD scales linearly with time *t*, is not fully reached even in the last time window of the 130 ps simulation. This makes difficult a reliable estimation of the self-diffusivity of the cations and anions. Yet, at least an indication of the diffusivities can be attempted for both the ionic 3D mobilities (D^*) according to the typical Einstein's formula considering the slope of the MSD plot to have reached the beginning of the diffusion regime toward the end of the simulation

$$D^* = \frac{1}{6} \lim_{t \to \infty} \frac{\langle (\mathbf{R}_i(t) - \mathbf{R}_i(0))^2 \rangle}{t} \quad (2)$$

For times *t* sufficiently long, thus being the mean square displacement MSD = $\langle (\mathbf{R}_i(t) - \mathbf{R}_i(0))^2 \rangle$ the one computed only in the last part of the plot in Figure 5. Indeed, we observed that at least 10 ps are needed to approach the caging regime due to the local vibrations of the ionic species.

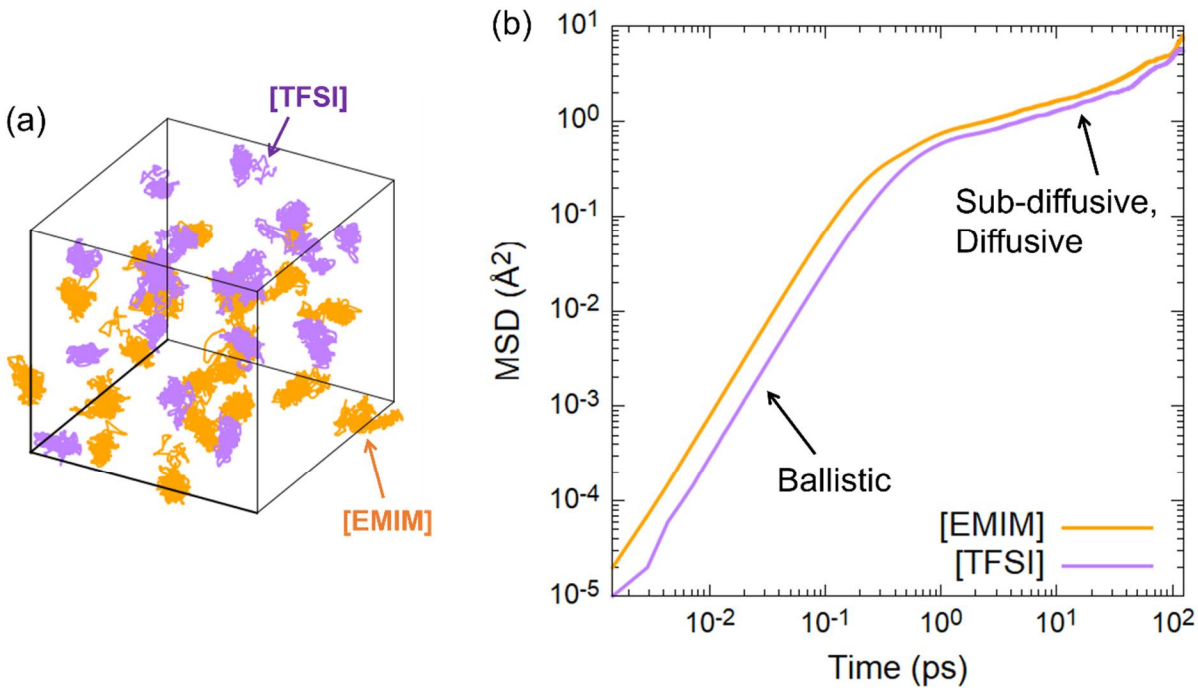

Figure 5. (a) Sketch of the trajectories of the center of mass of [EMIM] cations (orange) and [TFSI] anions (purple) during the simulation. (b) Mean square displacement (MSD) of the [EMIM] cations (orange line) and the [TFSI] anions (purple line) during the dynamics at 300 K. After the equilibration stage, represented by the initial slope, a mobility regime is reached and used to compute the ionic mobilities. Details are given in the text.

The estimated mobility coefficients are found to be close to the available experimental measurements[49,50] done with spin-echo technique. Specifically, we obtained mobility coefficients equal to 0.0070 Å^2/ps for the [EMIM] cation and of 0.0061 Å^2/ps for the [TFSI] anion, to be compared with the values of 0.007 and 0.004 Å^2/ps for the cation and the anion, respectively, measured[49,50] at room temperature. This is also an indication of the time scale required to get a realistic FPMD simulation of this class of systems able to reproduce with

acceptable accuracy slowly varying dynamical quantities. By looking into the details of the atomic structure of both the cation and the anion, we remark that, as shown in Figure 4, a predominance of trans conformers of the [TFSI] has been detected. Now, by analyzing the dynamics of the single molecules along the trajectory, we can see that a same molecule does not keep its configuration (either trans or cis) all along the motion of the IL but sometime undergoes spontaneous switch between the two isomers. A typical example representative of this trend is shown in Figure 6, where the isomers are discriminated based on the C-S-S-C torsion angle, as specified in paragraph 3.1, and indicate that there is only a small barrier separating the two isomers. Indeed, the system can overcome it with simple dynamical fluctuations during the 300 K NVT dynamics.

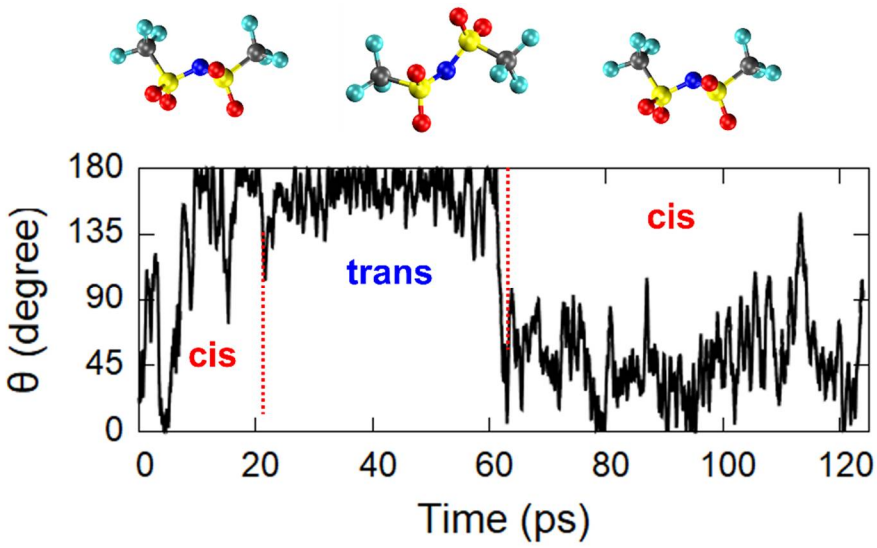

Figure 6. Evolution of the configuration of a typical [TFSI] molecule during the dynamics. The range of values around 180º of the C-S-S-C torsion angle indicate a trans conformer, whereas values in the range 25º-55º indicate a cis configuration.

In Figure 6, C-S-S-C angles around 180º indicate a trans configuration, whereas values in the range 25º-55º are referred to the cis isomer. The trajectories of C-S-S-C torsion angles of other [TFSI] molecules are also shown in Fig. S7 of the *Supporting information*, where an analogous analysis for the [EMIM] cation is reported for completeness in Fig. S8 in *Supporting Information*. The results show the ethyl group rotates around the bond with the imidazolium ring constantly, indicating the presence of a negligible energy barrier to this conformer change. As a general observation, we can infer that it might take even longer times than the one afforded here to observe a statistically meaningful number of conformational switches (here limited to two) to reproduce the actual experimental condition. Nonetheless, these processes are correctly captured in our simulations. To better quantify the free energy barrier for the switch between cis and trans configurations of the [TFSI], we resorted to blue moon ensemble (BME) simulations[51]. By using as a reaction coordinate the torsion angle C-S-N-S, which is able to discriminate between the two conformers, we performed auxiliary BME simulations with this reaction coordinates, starting from the NVT well equilibrated system. The results are summarized in Figure 7. In the free energy profile of Figure 7, each point, evidenced by black circles along the line, represents a sampled value of the C-S-N-S torsion angle (reaction coordinate), for which the BME simulation lasted for about 2 ps, necessary to get well averaged constraint forces for the thermodynamical integration. The range of sampled values, from 109º to 180º, spans all the torsion angles going from a trans to a cis conformer of the [TFSI] moiety.

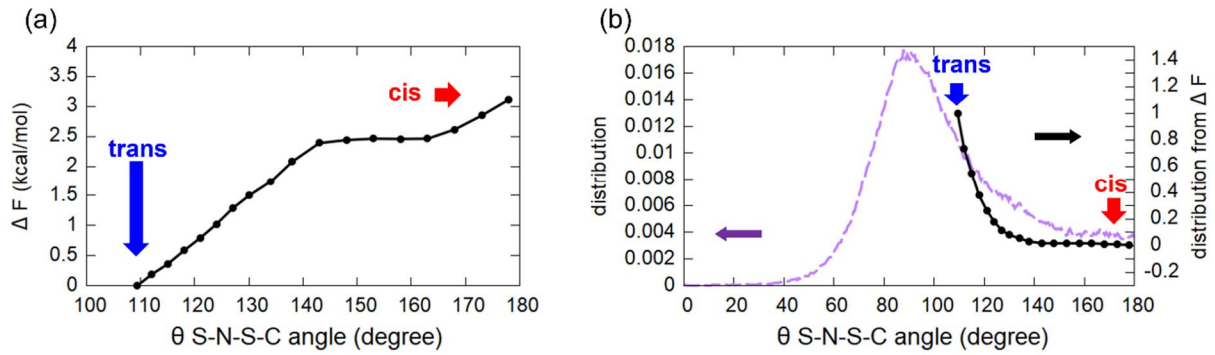

Figure 7. The left panel show the free energy profile along the S-N-S-C torsion angle (reaction coordinate) as obtained from the BME simulations. The right panel shows the distribution of the torsion angle S-N-S-C as obtained from the analysis of the unconstrained FPMD. The results of the BME simulation, in terms of $\exp(-\Delta F/k_B T)$, are shown for comparison.

As evidenced by this BME analysis, a free energy barrier of about 3.1 kcal/mol separates the trans from the cis configuration, sufficiently small to be overcome during our regular (unconstrained) NVT dynamics by simple statistical fluctuations. In fact, by computing from the free energy profile ΔF the corresponding probability as $\exp(-\Delta F/k_B T)$, being k_B the Boltzmann constant and T the simulation temperature, we get a curve that can be superposed to the statistical distribution almost exactly.

3.3 Electronic properties

Being the electronic structure of the system available simultaneously with the atomic configuration in a FPMD approach, we computed the Kohn-Sham eigenstates of the average

configuration of the liquid at 300 K. More precisely, in the Hamiltonian diagonalization procedure, to the occupied states, regularly updated in a FPMD approach, we added the lowest twelve unoccupied states. The result is sketched in Figure 8.

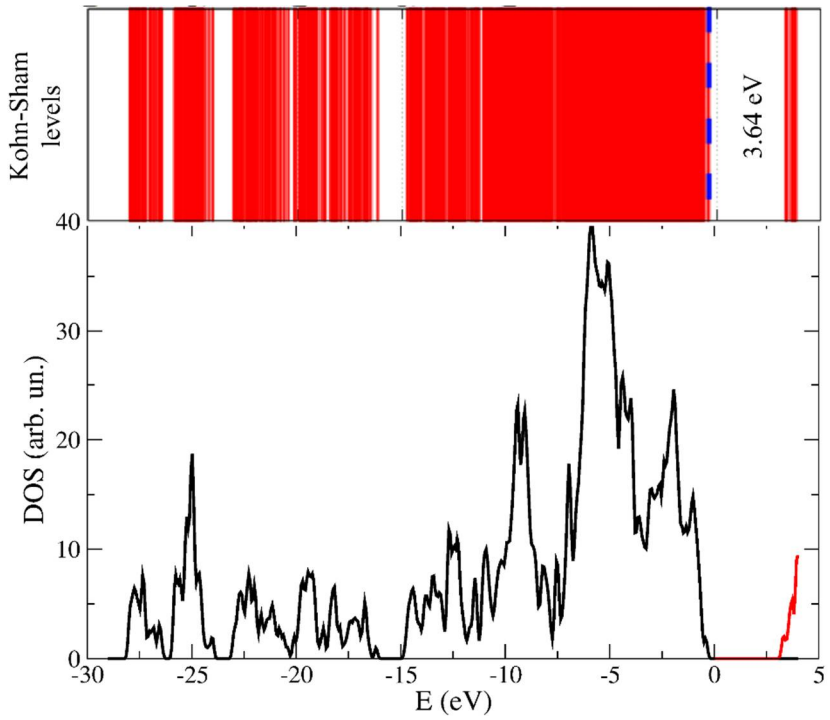

Figure 8. Band diagram and related electronic density of states (DOS) for the simulated [EMIM] [TFSI] ionic liquid. In the DOS (lower panel) the black line indicates the occupied states, whereas the red line the empty states. An energy gap of 3.64 eV separates the two set of Kohn-Sham eigenstates.

Within the computational approach used here and taking into consideration the systematic underestimation affecting DFT based calculations, an energy gap of 3.64 eV separates the top of the valence band from the bottom of the empty states. This gap does not undergo any noticeable shrinking all along the dynamics, thus keeping a wide energetic separation between the highest

occupied orbitals (HOMO) in proximity of the valence band upper edge and the lowest unoccupied orbitals (LUMO). On the other hand, the nature of the HOMO and LUMO orbitals differs significantly as shown in Figure 9. Specifically, the HOMO wavefunctions resemble a bonding state of the [TFSI] anion between the N and S atoms, with a pronounced amplitude located along the bond directions joining the central N and the two S atoms. Large contributions from the nearby O 2p states are also present (see Figure 9) as lobes localized on top of the oxygen atoms. Conversely, the LUMO states are localized [EMIM] cation and resemble mostly C-N antibonding states with wavefunctions carrying a node in the center of each C-N bond of the central pentagonal ring.

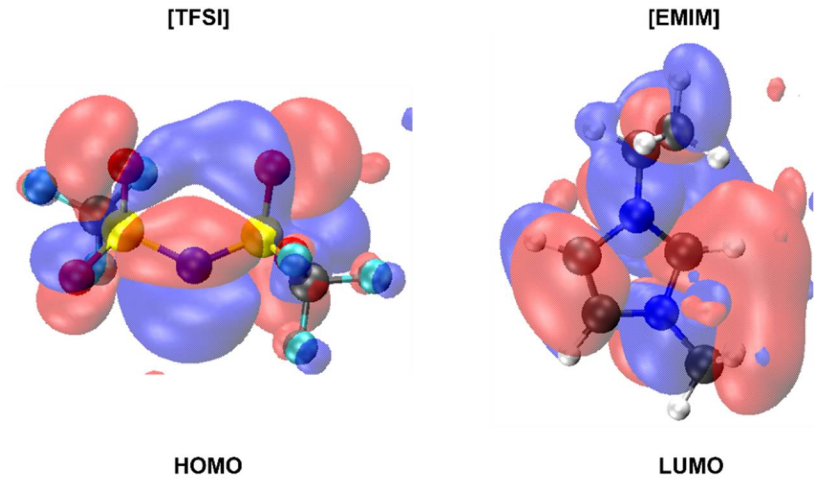

Figure 9. Typical highest occupied orbital (HOMO) and lowest unoccupied one (LUMO) in the ionic liquid. The top of the valence band is composed mostly of bonding states located on the N and S atoms of the anion [TFSI] with large contributions from the O 2p states visible as pronounced lobes in the left panel of the figure. Instead, the LUMO states resemble mostly C-N antibonding states of the [EMIM] cation with wavefunctions presenting a node in the center of

this chemical bond. Blue (negative amplitude) and red (positive amplitude) isosurfaces are shown at a value of 10^{-4} Å$^{-3/2}$.

To quantify the partial charges of each atom, we exploited the electronic density, available on the fly all along the dynamics, and computed for several uncorrelated configurations the value of the Bader charges[52,53] of each atom composing the cation and the anion of the IL. The result of this analysis is reported in Figure 10.

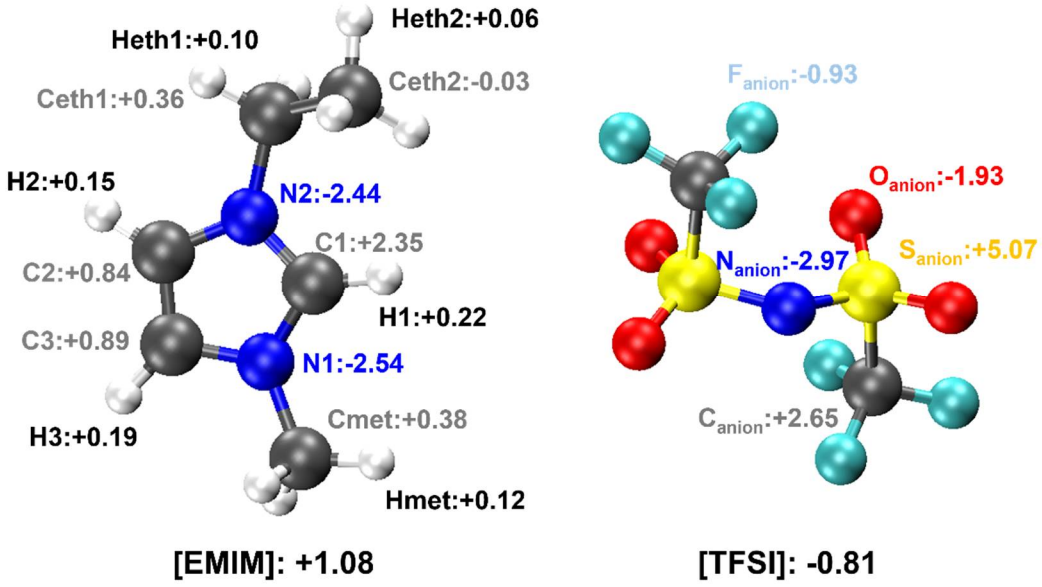

Figure 10. Schematic representation of the Bader charge of the atoms of the [EMIM] and [TFSI] ions. The color code of the atoms and their labeling is identical to all former figures.

The main features can be summarized in: (i) the Bader charges of each atom does not undergo any significant fluctuation all along the dynamics, (ii) the Bader charges of the [TFSI] anion are

unaffected by the configuration of the molecule in the sense that both the cis and the trans conformers are characterized by the same values within the numerical accuracy allowed by this type of computational approach. For the sake of completeness, the Bader charges of the cis and trans [TFSI] anion in the gas phase are reported in Figure S9 of the Supporting *Information*. And (iii) the total Bader charge of the [EMIM] is equal to +1.08 *e* and the one of the [TFSI] is -0.81 *e*, confirming the cationic and anionic nature of the two moieties as a whole and the detailed distribution of the partial charges contributing to this overall values. A unitary rotation of the Kohn-Sham orbitals within the maximally localized Wannier function and Wannier functions centers (WFCs) scheme[54,55], allows for a very practical analysis of the chemical bonds and provide a shorthand visualization of the electronic structure that can result more cumbersome by resorting uniquely on the Kohn-Sham orbitals. A picture of the WFCs for the whole [EMIM] and [TFSI] ions is shown in Figure S10 of the *Supporting Information*. Here, we limit the discussion to the peculiarity of the S-O[56] and C-F[57] chemical bonds. In terms of distribution of the WFCs around the atoms of interest, the situation is shown in Figure 11.

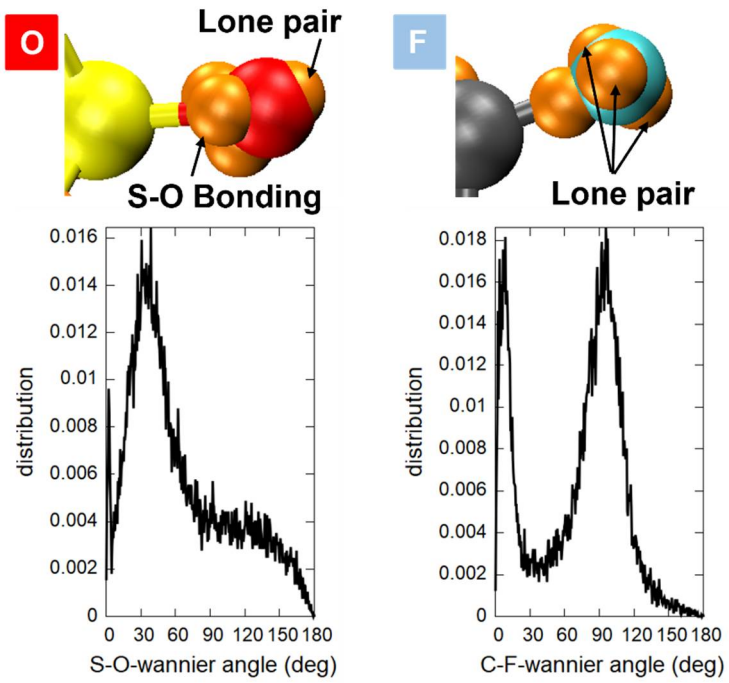

Figure 11. Wannier functions centers (orange spheres) and their distribution around the S-O (left panel) and the C-F (right panel) chemical bonds monitored during the FPMD dynamics. If the angles are small, this means that the Wannier functions centers are located along the bonds.

The structure and nature of S-O chemical bonds has been a source of debate and only in the early 1950's some consensus could be eventually reached. In short, a sort of compromise[56] exists between the electronegative O atoms and the need for stable S valence electrons. In the case of the sulfur dioxide-like groups of [TFSI], the O atoms show basically a single lone pair remaining bound to the O atoms and three WFCs more or less displaced toward the S atom, but nonetheless close to O, thus conferring an ionic character to this bond and accounting for a positive charge left on top of the S atom. A positive charge left on the sulfur is indeed the result expected on the basis of an accurate atomic orbital analysis in Ref. 56 for sulfones and

sulfoxides and in line with the localization of the WFCs in the present analysis (Figure 11) and also compatible with the Bader charges analysis reposted in Figure 10. The S-O bond is then very strong, resembling a tight double bond but being mainly ionic with the (negative) valence electrons mostly displaced toward the O site. Less complicated is the situation of the C-F bond. In this case three WFCs remain as lone pairs in proximity of the F site, whereas one doubly occupied WFC is located along the C-F bond (see Figure 11) but strongly displaced toward the F site (see Figure S11 in *Supporting Information*), thus accounting for a negative partial charge of F, as opposed to a positive one on C, in perfect agreement with the Bader charges analysis. The details of other WFCs are reported in Figure S12 of the *Supporting Information*.

The availability of the WFCs is also a useful tool to compute the local dipole moment **p** of each [EMIM][TFSI] pair of the IL as a simple sum of point-like charges

$$\mathbf{p} = \sum_I Z_I \mathbf{R}_I - \sum_i f_i \, \mathbf{r}_i^{WFC} \qquad (3)$$

where Z_I is the valence charge of the I^{th} atom, $\mathbf{R}_I$ its cartesian position in the simulation cell, f_i the occupation number of the i^{th} Wannier orbital or center (f_i=2 in a spin restricted approach or 1 in a spin unrestricted calculation) and $\mathbf{r}_i^{WFC}$ the position of the i^{th} Wannier function center. We recall that the only gauge invariant dipole that has a physical meaning[59] in a globally neutral simulation cell is the one between the EMIM cation and the TFSI anion. We performed this analysis on our system by computing the dipole moments between each [EMIM]-[TFSI] pair in our simulation cell. According to the PCF between [EMIM] and [TFSI] (Figure 2), the first coordination shell has an average radius of ~9.3 Å. On these grounds, the dipole moments of [EMIM]-[TFSI] dimers were calculated according to the criterion that its center-of-mass distance is lower than 9.3 Å. A representative snapshot of an [EMIM] and one surrounding

[TFSI] in the first coordination shell is shown in panel (a) of Figure 12 and the related coordination number in this first coordination number is around 7~8 (see Figure S13 in *Supporting Information*). Panel (b) of Figure 12 shows the distribution of the dipole moment in the ionic liquid. The average value of the dipole moment is 33.0 D, significantly larger than the values computed for an isolated dimer [EMIM][TFSI] in the gas phase (16.1 D for [EMIM]-*cis* [TFSI] and 20.3 D for [EMIM]-*trans* [TFSI] dimers). This enhanced value is not an unexpected effect in an extended polar liquid, where the presence of H-bonds of surrounding ions enhances the electrostatic interaction between [EMIM] and [TFSI].

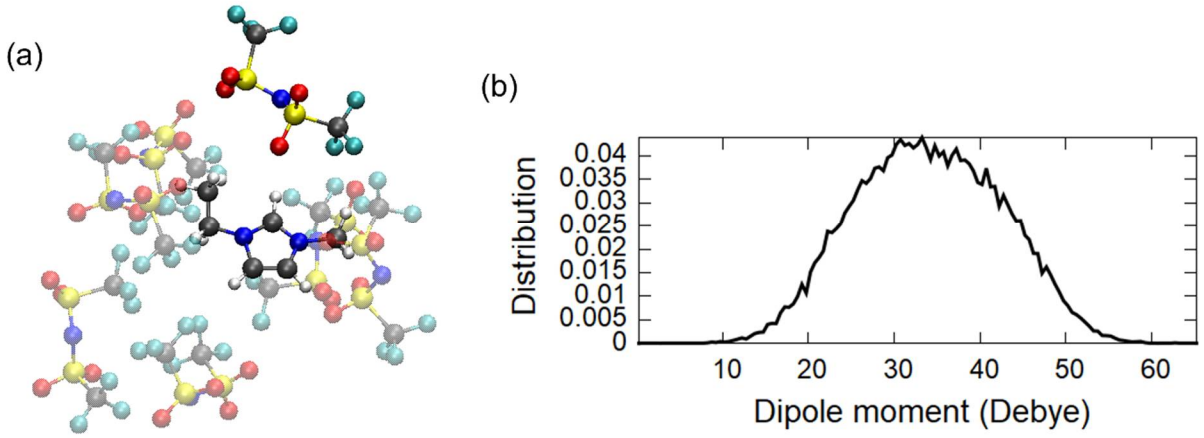

Figure 12. (a) Typical geometry of one [EMIM] and its surrounding [TFSI] in the first coordination shell. (b) Dipole moment distribution of the [EMIM]-[TFSI] pairs (first coordination shell) inside the ionic liquid.

Since the dipole moment of an ionic liquid is experimentally difficult to measure[58], this can provide a useful quantitative analysis complementing experimental probes. Yet, a closer contact with experiments would be desirable. To encompass this difficulty, since the global dipole

moment **M**(t) is available all along the dynamical trajectory, we computed the infra-red (IR) spectrum as the Fourier transform of the dipole-dipole autocorrelation function,

$$\alpha(\omega) = \frac{4\pi \tanh\left(\beta\hbar\omega/2\right)}{3\hbar c V n(\omega)} \int_0^\infty e^{-i\omega t} \langle \mathrm{M}(t)\mathrm{M}(0)\rangle dt \qquad (4)$$

Where β=1/$k_B T$, being T the simulation temperature of our NVT simulation, c the speed of light, V the volume of the simulation cell, and $n(\omega)$: refractive index; the brackets indicate autocorrelation function. We recall that the IR absorption constant $\alpha(\omega)$ is related to the imaginary part of the refractive index $\varepsilon_2(\omega)$ by the relation $\varepsilon_2(\omega) = c\ \alpha(\omega)/2\omega$. The IR spectrum has the advantage that has been experimentally detected[59], thus allowing for a direct comparison, and computed within quantum chemical approaches comparable to the one used here[60]. Equally important is the dielectric function $\varepsilon_1(\omega)$ of the ionic liquid[61], since it is a key parameter determining the solvation properties of the IL and a probe of the response of the system to an applied electric field, thus directly useful for the realization of devices. To extract this information, we make use of the well-known Kramers-Kronig relations[62,63]

$$\varepsilon_1(\omega) = 1 + \frac{2}{\pi} P \int_0^\infty \frac{\omega' \cdot \alpha(\omega)}{\omega'^2 - \omega^2}\, d\omega' \qquad (5)$$

The computed IR spectrum and accompanying dielectric function are shown in Figure 13. Consistently with the experimental outcome[59,60], our computed IR spectrum (lower panel in Figure 13) is dominated by the contribution of [TFSI] and we are able to reproduce all the sharp peaks between 500 and 1500 cm^{-1}, attributed to all the ring modes as detailed in Ref. 60. Analogously, the small peak between 2800 and 3100 cm^{-1}, originating from the C-H stretching modes, are just a small contribution.

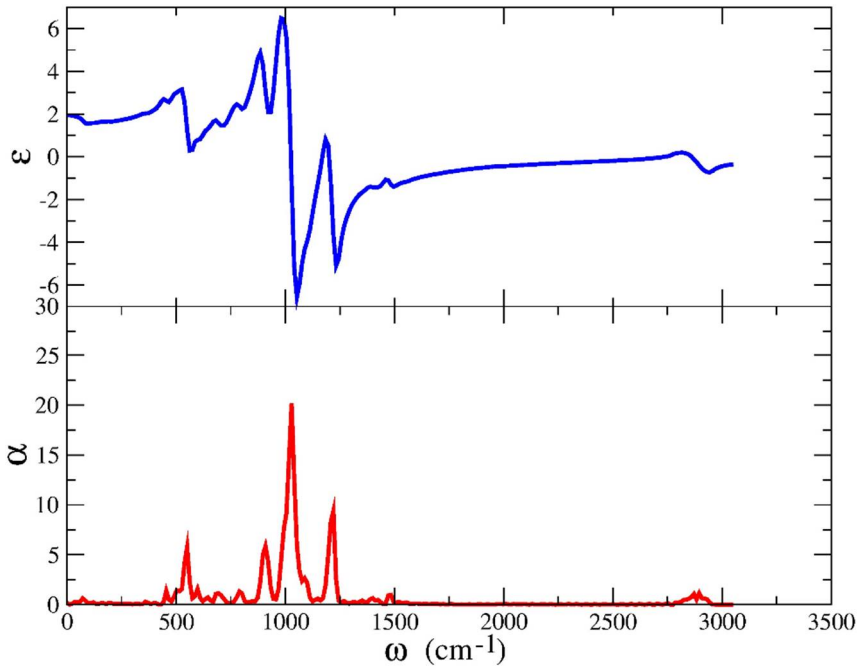

Figure 13. The real part of refractive index (ε_1) and the IR absorption spectrum (α) of the simulated [EMIM][TFSI] as obtained from the autocorrelation function of the total dipole moment as described in the text.

To disentangle the contributions of each vibrational mode to the IR spectrum, we performed a normal modes analysis of an [EMIM]-cis[TFSI] dimer. These results are summarized in Table S1 in *Supporting Information*. We can observe that a slight shift toward lower frequencies, affecting particularly this part of our IR spectrum, is not surprising and represent a typical limit in DFT-based calculations of IR response in polar liquids[64]. The dielectric function, on the other hand, provides useful information about the frequency range in which the material is operational and allows to tune the current flow upon an applied electric field, a key issue in the fabrication of field-effect transistors exploiting ILs.

CONCLUSIONS

We undertook a thorough analysis of structural, dynamical, electronic and spectroscopical properties of the ionic liquid [EMIM][TFSI], representing a current target system for the realization of next-generation electronic devices. By resorting to long-lasting FPMD simulations, we unravel the highly dynamical yet tunable features of the system, providing a microscopic picture not accessible to experimental probes. In particular, we evidence how the diffusion is a slow process, whereas fast conformational changes occur at room temperature without affecting the overall structure of the polar liquid, which indeed presents pair correlation functions that do not undergo significant change on the simulation time scale afforded here.

The efficient H-bond network realized inside the IL, is responsible for an enhancement of the local dipole moment of the [EMIM][TFSI] pairs that, in turn, confers a remarkable stability to this peculiar liquid phase. This is encouraging in view of the use of these liquid material in devices that are expected to operate at room temperature. The electronic structure is characterized by a rather large band gap, ensuring absence of undesired HOMO-LUMO transitions at the typical working conditions. On the other hand, an analysis of the IR response of the system and the related dielectric function provides insightful information on the best suited range of frequencies where the material can be safely employed, contributing to an eco-efficient realization of nanotechnological devices.

ASSOCIATED CONTENT

Supporting Information. Additional figures and data mentioned in the text. The following files are available free of charge: supporting_information.PDF

AUTHOR INFORMATION

Corresponding Authors

E-mail: kana.ishisone@ipcms.unistra.fr

E-mail: mauro.boero@ipcms.unistra.fr

ORCID:

Kana Ishisone: 0000-0001-6637-5604

Mauro Boero: 0000-0002-5052-2849

Author Contributions

The manuscript was written through contributions of all authors. All authors have given approval to the final version of the manuscript.

Funding Sources

K. I. is funded by the French Bourse du Gouvernement - Ministère Affaires Étrangeres and the Japanese Takenaka Scholarship Foundation.

Notes

The authors declare no competing financial interest.

ACKNOWLEDGMENT

We thank the HPC Center at the University of Strasbourg funded by the Equipex Equip@Meso project (Programme Investissements d'Avenir) - CPER Alsacalcul/Big Data, and the Grand Equipement National de Calcul Intensif (GENCI) under allocation DARI-A0100906092. We are grateful to Iréné Amiehe Essomba for his kind help in the preparation of the ILs system, and to Emanuele Orgiu and Carlo Massobrio for fruitful discussions and insightful suggestions.

REFERENCES

(1) Ye, J. T.; Zhang, Y. J.; Akashi, R.; Bahramy, M. S.; Arita, R.; Iwasa, Y. Superconducting Dome in a Gate-Tuned Band Insulator. *Science* **2012**, *338*, 1193-1196.

(2) Costanzo, D.; Jo, S.; Berger, H.; Morpurgo, A. F. Gate-induced superconductivity in atomically thin MoS_2 crystals. *Nature Nanotech*. **2016**, *11*, 339-344.

(3) Jia, C.; Famili, M.; Carlotti, M.; Liu, Y.; Wang, P.; Grace, I. M.; Feng, Z.; Wang, Y.; Zhao, Z.; Ding, M.; Xu, X.; Wang, C.; Lee, S.-J.; Huang, Y.; Chiechi, R. C.; Lambert, C. J.; Duan, X. Quantum interference mediated vertical molecular tunneling transistors. *Sci. Adv*. **2018**, *4*, eaat8237.

(4) Upadhyay, N. K.; Jiang, H.; Wang, Z.; Asapu, S.; Xia, Q.; Yang, J. J. Emerging Memory Devices for Neuromorphic Computing. *Adv. Mater. Technol*. **2019**, *4*, 1800589.

(5) John, R. A.; Liu, F.; Chien, N. A.; Kulkarni, M. R.; Zhu, C.; Fu, Q.; Basu, A.; Liu, Z.; Mathews, N. Synergistic Gating of Electro-Iono-Photoactive 2D Chalcogenide Neuristors: Coexistence of Hebbian and Homeostatic Synaptic Metaplasticity. *Adv. Mater*. **2018**, *30*, 1800220.

(6) Gao, G.; Yu, J.; Yang, X.; Pang, Y.; Zhao, J.; Pan, C.; Sun, Q.; Wang, Z. L. Triboiontronic Transistor of MoS_2. *Adv. Mater*. **2018**, *31*, 1806905.

(7) Kelly, A. G.; Hallam, T.; Backes, C.; Harvey A.; Esmaeily, A. S.; Godwin, I; Coelho, J.; Nicolosi, V; Lauth J.; Kulkarni A.; Kinge S.; Siebbeles L. D. A.; Duesberg G. S.; Coleman J. N. All-printed thin-film transistors from networks of liquid-exfoliated nanosheets. *Science* **2017**, *356*, 69-73.

(8) Park, S. J.; Nam, D.; Jeon, D.-Y.; Kim, G.-T. Transport-map analysis of ionic liquid-gated ambipolar WSe_2 field-effect transistors. *Semicond. Sci. Technol.* **2019**, *34*, 075022.

(9) Huang, J.-K.; Pu, J.; Hsu, C.-L.; Chiu, M.-H.; Juang, Z.-Y.; Chang, Y.-H.; Chang, W.-H,; Iwasa, Y.; Takenobu, T.; Li, L.-J. Large-Area Synthesis of Highly Crystalline WSe_2 Monolayers and Device Applications. *ACS Nano* **2014**, *8*, 923-930.

(10) Umebayashi, Y.; Fujimori, T.; Sukizaki, T.; Asada, M.; Fujii, K.; Kanzaki, R.; Ishiguro, S. Evidence of Conformational Equilibrium of 1-Ethyl-3-methylimidazolium in Its Ionic Liquid Salts: Raman Spectroscopic Study and Quantum Chemical Calculations. *J. Phys. Chem. A* **2005**, *109*, 40, 8976-8982.

(11) Dhumal, N. R.; Kim, H. J.; Kiefer, J. Electronic Structure and Normal Vibrations of the 1-Ethyl-3-methylimidazolium Ethyl Sulfate Ion Pair. *J. Phys. Chem. A* **2011**, *115*, 15, 3551-3558.

(12) Fujii, K.; Soejima, Y.; Kyoshoin, Y.; Fukuda, S.; Kanzaki, R.; Umebayashi, Y.; Yamagichi, T.; Ishiguro, S.; Takamuku, T. Liquid Structure of Room-Temperature Ionic Liquid, 1-Ethyl-3-methylimidazolium Bis-(trifluoromethanesulfonyl) Imide. *J. Phys. Chem. B* **2008**, *112*, 14, 4329–4336.

(13) Liang, Z.; Zhao, C.; Zhao, W.; Zhang, Y.; Srimuk, P.; Presser, V.; Feng, G. Molecular Understanding of Charge Storage in MoS_2 Supercapacitors with Ionic Liquids. *Energy & Environ. Materials* **2021**, *4*, 631-637.

(14) Zhao, W.; Bi, S.; Zhang, C.; Rack, P.D.; Feng, G. Adding Solvent into Ionic Liquid-Gated Transistor: The Anatomy of Enhanced Gating Performance. *ACS Appl. Mater. Interfaces* **2019** *11*, 13822-13830.

(15) Vioux, A.; Coasne, B. From Ionogels to Biredox Ionic Liquids: Some Emerging Opportunities for Electrochemical Energy Storage and Conversion Devices. *Adv. Energy Mater.* **2017**, *7*, 1700883.

(16) Schlaich, A.; Jin, D.; Bocquet, L.; Coasne, B., Electronic screening using a virtual Thomas–Fermi fluid for predicting wetting and phase transitions of ionic liquids at metal surfaces. *Nature Mater*. **2021**, 1-9. DOI 10.1038/s41563-021-01121-0

(17) Ori, G.; Massobrio, C.; Pradel, A.; Ribes, M.; Coasne, B. Structure and Dynamics of Ionic Liquids Confined in Amorphous Porous Chalcogenides. *Langmuir* **2015**, *31*, 6742-6751.

(18) Costa, S. P. F.; Azevedo, A. M. O.; Pinto, P. C. A. G.; Saraiva, M. L. M. F. S. Environmental Impact of Ionic Liquids: Recent Advances in (Eco)toxicology and (Bio) degradability. *ChemSusChem* **2017**, *10*, 2321-2347.

(19) Frade, R. F.; Afonso, C. A. Impact of ionic liquids in environment and humans: An overview. *Hum. Exp. Toxicol*. **2010**, *29*, 1038-1054.

(20) Klein, J. M.; Panichi, E.; Gurkan, B. Potential dependent capacitance of [EMIM][TFSI], [N_{1114}][TFSI] and [PYR_{13}][TFSI] ionic liquids on glassy carbon. *Phys. Chem. Chem. Phys.* **2019**, *21*, 3712-3720.

(21) Yuan, C.; Zhu, X.; Su, L.; Yang, D.; Wang, Y.; Yang, K.; Cheng, X. Preparation and characterization of a novel ionic conducting foam-type polymeric gel based on polymer PVdF-HFP and ionic liquid [EMIM][TFSI]. *Colloid Polym Sci* **2015**, *293*, 1945-1952.

(22) Höfft, O.; Bahr, S.; Himmerlich, M.; Krischok, S.; Schaefer, J. A.; Kempter, V. Electronic Structure of the Surface of the Ionic Liquid [EMIM][Tf_2N] Studied by Metastable Impact Electron Spectroscopy (MIES), UPS, and XPS. *Langmuir* **2006**, *22*, 7120-7123.

(23) Reichert, W. M.; Holbrey, J. D.; Swatloski, R. P.; Gutowski, K. E.; Visser, A. E.; Nieuwenhuyzen, M.; Seddon, K. R.; Rogers, R. D. Solid-State Analysis of Low-Melting 1,3-Dialkylimidazolium Hexafluorophosphate Salts (Ionic Liquids) by Combined X-ray Crystallographic and Computational Analyses. *Crystal Growth & Design* **2007**, *7*, 1106-1114.

(24) Bühl, M.; Chaumont, A.; Schurhammer, R.; Wipff, G. Ab Initio Molecular Dynamics of Liquid 1,3-Dimethylimidazolium Chloride. *J. Phys. Chem. B* **2005**, *109*, 39, 18591-18599.

(25) Wendler, K.; Brehm, M.; Malberg, F.; Kirchner, B.; Delle Site, L. Short Time Dynamics of Ionic Liquids in AIMD-Based Power Spectra. *J. Chem. Theory Comput*. **2012**, *8*, 1570-1579.

(26) Kohn, W.; Sham, L. J. Self-Consistent Equations Including Exchange and Correlation Effects. *Phys. Rev*. **1965**, *140*, A1133-A1138.

(27) Car, R.; Parrinello, M. Unified Approach for Molecular Dynamics and Density-Functional Theory. *Phys. Rev. Lett.* **1985**, 55, 2471-2474.

(28) CPMD, copyright IBM Corp. (1990–2021), copyright MPI für Festkörperforschung Stuttgart (1997–2001). www.cpmd.org

(29) Troullier, N.; Martins, J. L. Efficient pseudopotentials for plane-wave calculations. *Phys. Rev. B* **1991**, *43*, 1993-2006.

(30) Troullier, N.; Martins, J. L. Efficient pseudopotentials for plane-wave calculations. II. Operators for fast iterative diagonalization. *Phys. Rev. B* 1991, *43*, 8861-8869.

(31) Becke, A. D. Density-functional exchange-energy approximation with correct asymptotic behavior. *Phys. Rev. A* **1988**, *38*, 3098–3100.

(32) Lee, C.; Yang, W.; Parr, R. G. Development of the Colle-Salvetti correlation-energy formula into a functional of the electron density. *Phys. Rev. B* **1988**, *37*, 785–789.

(33) Silvestrelli, P. L. Van der Waals interactions in DFT made easy by Wannier functions. *Phys. Rev. Lett*. **2008**, *100*, 053002.

(34) Ikeda, T.; Boero, M. Role of van der Waals corrections in first principles simulations of alkali metal ions in aqueous solutions. *J. Chem. Phys*. **2015**, *143*, 194510.

(35) Nosé, S. A molecular dynamics method for simulations in the canonical ensemble. *Mol. Phys*. **1984**, 52, 255-268.

(36) Nosé, S. A unified formulation of the constant temperature molecular dynamics methods. *J. Chem. Phys.* **1984**, *81*, 511-519

(37) Hoover, W. G. Canonical dynamics: Equilibrium phase-space distributions. *Phys. Rev. A* **1985**, *31*, 1695-1697.

(38) Jacquemin, J.; Husson, P.; Padua, A. A. H.; Majer, V. Density and viscosity of several pure and water-saturated ionic liquids. *Green Chem.* **2006**, *8*, 172-180.

(39) Fredlake, C. P.; Crosthwaite, J. M.; Hert, D. G.; Aki, S. N. V. K.; Brennecke, J. F. Thermophysical Properties of Imidazolium-Based Ionic Liquids. *J. Chem. Eng. Data* **2004**, *49*, 954-964.

(40) Canongia Lopes, J. N.; Deschamps, J.; Pádua, A. A. H. Modeling Ionic Liquids using a Systematic All-Atom Force Field. *J. Phys. Chem. B* **2004**, *108*, 2038-2047.

(41) Köddermann, T.; Paschek, D.; Ludwig, R. Molecular Dynamic Simulations of Ionic Liquids: A Reliable Description of Structure, Thermodynamics and Dynamics. *ChemPhysChem* **2007**, *8*, 2464− 2470.

(42) Magyar, R. J.; Root, S.; Mattsson, T. R. Equations of state for mixtures: results from density-functional (DFT) simulations compared to high accuracy validation experiments on Z. *J. Phys.: Conf. Ser.* **2014**, *500*, 162004.

(43) Rousseau, R.; Boero, M.; Bernasconi, M.; Parrinello, M.; Terakura, K. Ab initio Simulation of Phase Transitions and Dissociation of H_2S at High Pressure. *Phys. Rev. Lett.* **2000**, *85*, 1254-1257.

(44) Rotnicki, K.; Sterczyńska, A.; Fojud, Z.; Jażdżewska, M.; Beskrovnyi, A.; Waliszewski, J.; Śliwińska-Bartkowiak, M. Phase transitions, molecular dynamics and structural properties of 1-Ethyl-3-methylimidazolium bis(trifluoromethylsulfonyl)imide ionic liquid. *J. Mol. Liq.* **2020**, *313*, 113535.

(45) Galy, J.; Matar, S. F. Electron Lone-Pairs Stereochemistry and Drastic van der Waals and Pressure Effects in AsF_3 from First Principles. *Condens. Matter* **2021**, *6*, 31.

(46) Ori, G.; Villemot, F.; Viau, L.; Vioux, A; Coasne, B. Ionic liquid confined in silica nanopores: molecular dynamics in the isobaric–isothermal ensemble. *Mol. Phys.* **2014**, *112*, 1350-1361.

(47) Lassègues, J. C.; Grondin, J.; Holomb, R.; Johansson, P. Raman and *ab initio* study of the conformational isomerism in the 1-ethyl-3-methyl-imidazolium bis(trifluoromethanesulfonyl)imide ionic liquid. *J. Raman Spectrosc*. **2007**, *38*, 551-558.

(48) Holbrey, J. D.; Reichert, W. M.; Rogers, R. D. Crystal structures of imidazolium bis(trifluoromethanesulfonyl)imide 'ionic liquid' salts: the first organic salt with a cis-TFSI anion conformation. *Dalton Trans*. **2004**, *1*, 2267-2271.

(49) Noda, A.; Hayamizu, K.; Watanabe, M. Pulsed-Gradient Spin−Echo ^{1}H and ^{19}F NMR Ionic Diffusion Coefficient, Viscosity, and Ionic Conductivity of Non-Chloroaluminate Room-Temperature Ionic Liquids. *J. Phys. Chem. B* **2001**, *105*, 4603-4610.

(50) D'Agostino, C.; Mantle, M. D.; Mullan, C. L.; Hardacre, C.; Gladden, L. F. Diffusion, Ion Pairing and Aggregation in 1-Ethyl-3-Methylimidazolium-Based Ionic Liquids Studied by ^{1}H and ^{19}F PFG NMR: Effect of Temperature, Anion and Glucose Dissolution. *ChemPhysChem* **2018**, *19*, 1081-1088.

(51) Sprik, M; Ciccotti, G. Free eneregy from constrained molecular dynamics. *J. Chem. Phys*. **1998**, *109*, 7737-7744.

(52) Bader, R. F. W. A quantum theory of molecular structure and its applications. *Chem. Rev*. **1991**, *91*, 893–928.

(53) Henkelman, G.; Arnaldsson, A.; Jónsson, H. A fast and robust algorithm for Bader decomposition of charge density. *Comput. Mater. Sci.* **2006**, *36*, 354-360.

(54) Marzari, N.; Vanderbilt, D. Maximally localized generalized Wannier functions for composite energy bands. *Phys. Rev. B* **1997**, *56*, 12847-12865.

(55) Resta, R. Quantum-Mechanical Position Operator in Extended Systems. *Phys. Rev. Lett*. **1998**, *80*, 1800-1803.

(56) Moffitt, W. The Nature of the Sulphur-Oxygen Bond. *Proc. of the Royal Soc. of London. Series A, Math. and Phys. Sci.* **1950**, *200*, 409-428.

(57) O'Hagan, D. Understanding organofluorine chemistry. An introduction to the C–F bond. *Chem. Soc. Rev*. **2008**, *37*, 308-319.

(58) Wendler, K., Zahn, S.; Dommert, F.; Berger, R.; Holm, C.; Kirchner, B.; Delle Site, L. Locality and Fluctuations: Trends in Imidazolium-Based Ionic Liquids and Beyond. *J. Chem. Theory Comput.* **2011**, *7*, 3040–3044.

(59) Kiefer, J.; Fries, J.; Leipertz, A. Experimental Vibrational Study of Imidazolium-Based Ionic Liquids: Raman and Infrared Spectra of 1-Ethyl-3-methylimidazolium Bis(trifluoromethylsulfonyl)imide and 1-Ethyl-3-methylimidazolium Ethylsulfate. *Appl. Spectroscopy* **2007**, *61*, 1306-1311.

(60) Eilmes, A.; Kubisiak, P.; Brela, M. Explicit Solvent Modeling of IR and UV−Vis Spectra of 1-Ethyl-3-methylimidazolium Bis(trifluoromethylsulfonyl)imide Ionic Liquid. *J. Phys. Chem. B* **2016**, *120*, 11026−11034.

(61) Huang, M.-M.; Jiang, Y.; Sasisanker, P.; Driver, G. W.; Weingärtner, H. Static Relative Dielectric Permittivities of Ionic Liquids at 25 ºC. *J. Chem. Eng. Data* **2011**, *56*, 1494–1499.

(62) Kronig, R. de L. On the theory of the dispersion of X-rays. *J. Opt. Soc. Am.* **1926**, *12*, 547–557.

(63) Kramers, H. A. La diffusion de la lumière par les atomes. *Atti Cong. Intern. Fisica* (Transactions of Volta Centenary Congress) **1927**, *2*, 545–557.

(64) Schmidt, D. A.; Scipioni, R.; Boero, M. Water Solvation Properties: An Experimental and Theoretical Investigation of Salt Solutions at Finite Dilution. *J. Phys. Chem. A* **2009**, *113*, 7725–7729.

SYNOPSIS (Word Style “SN_Synopsis_TOC”).

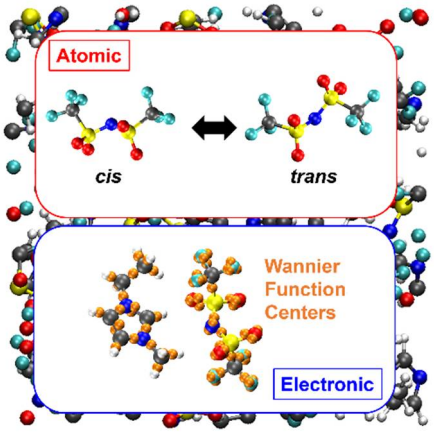

[EMIM][TFSI]